



# Nonuniform compensation of current density distribution in polymer electrolyte fuel cells by local heating

Shangwei Zhou<sup>a</sup>, Lara Rasha<sup>a,c</sup>, Linlin Xu<sup>a,b</sup>, Wenjia Du<sup>a,c</sup>, Paul.R. Shearing<sup>a,c,d</sup>, Marc-Olivier Coppens<sup>b</sup>, Dan J.L. Brett<sup>a,c</sup>, Rhodri Jervis<sup>a,c,\*</sup>

<sup>a</sup> Electrochemical Innovation Lab, Department of Chemical Engineering, University College London, London WC1E 7JE, United Kingdom

<sup>b</sup> EPSRC "Frontier Engineering" Centre for Nature Inspired Engineering & Department of Chemical Engineering, University College London, London WC1E 7JE, United Kingdom

<sup>c</sup> The Faraday Institution, Quad One, Harwell Science and Innovation Campus, Didcot OX11 0RA, United Kingdom

<sup>d</sup> Department of Engineering Science, University of Oxford, Parks Road, Oxford OX1 3PJ, United Kingdom

## ARTICLE INFO

### Keywords:

Polymer Electrolyte Fuel Cell (PEFC)  
Thermal management  
Current density distribution mapping  
Temperature distribution mapping  
Local heating

## ABSTRACT

A homogeneous current density distribution improves a fuel cell's performance and prolongs its service life. Effective cell structure designs and uniform compression during assembly could support this goal by ensuring a homogeneous reaction rate across the activation area. Due to the coupling of hydro-electro-thermal relationships, for instance, the concentration of reactants along the flow field decreases continuously as the electrochemical reaction proceeds, and the subsequent accumulation of liquid water leads to a low current density at the outlet. The effect of operating conditions, such as local heating, on the current density distribution requires further investigation. This paper studies the impact of local heating on polymer electrolyte fuel cell (PEFC) performance and analyses the effects on voltage by mapping the current density distribution across the active area. Local heating was supplied to the three regions of the electrode, namely, fuel inlet, central and outlet regions, with the latter exhibiting the best performance (in the activation, Ohmic and mass transport controlled region, the output voltage increases compared to no local heating corresponding to 1.28%, 2.17% and 2.46%, respectively). Here, we show that in all local heating cases, outlet heating can compensate for the lowest current density region with the largest current density increased by  $91.10 \text{ mA cm}^{-2}$  and achieves a more homogeneous current distribution, while inlet heating aggravates heterogeneity. This study provides practical guidance for optimal thermal management system development whereby the cooling channel design should be locally optimised for more uniform distributions of current density and temperature compared to heating the cell uniformly.

## 1. Introduction

Polymer electrolyte fuel cells (PEFCs) are considered one of the most promising next-generation power systems, with the potential to achieve high efficiency, environmentally friendly operation, and independence from fossil fuels when operated with green hydrogen. However, manufacturing cost and service lifespan limit the commercialisation process of PEFCs [1–3]. Due to the variety of operational strategies (active/passive cooling), cell designs (flow field design) and materials, fuel cells exhibit complex hydro-electro-thermal characteristics, making it difficult to understand the coupled interaction between localised current and heat crucial for developing advanced systems. The nonuniform distribution of current densities results in heterogeneous

heat and water production, thus affecting reactant transport. This inhomogeneity can become increasingly prominent, leading to system performance degradation and, ultimately, reduced cell lifetime [4].

Measurement of the regionally dynamic current distribution by direct mapping can offer essential insight into the electrochemical reactions that happen inside. Experimental mapping techniques have been widely investigated to understand the root and mechanisms of inhomogeneity; Hwang et al. [5] constructed a segmented current collector with a  $4 \times 4$  array of Hall-effect current sensors and found that the uniformity increased with current reduction. Similarly, Yu et al. [6] upgraded to 36 individual resistors to explore the current density responses during the reactant starvation and shutdown process, and their results revealed that the local current response was inconsistent after

\* Corresponding author at: Electrochemical Innovation Lab, Department of Chemical Engineering, University College London, London WC1E 7JE, United Kingdom.  
E-mail address: [rhodri.jervis@ucl.ac.uk](mailto:rhodri.jervis@ucl.ac.uk) (R. Jervis).

<https://doi.org/10.1016/j.enconman.2023.117717>

Received 21 August 2023; Received in revised form 25 September 2023; Accepted 26 September 2023

Available online 29 September 2023

0196-8904/© 2023 The Authors. Published by Elsevier Ltd. This is an open access article under the CC BY license (<http://creativecommons.org/licenses/by/4.0/>).

applying a dummy load following shutdown to consume the residual gas in the channel and reduce the cell potential; therefore, a lower dummy load is preferable. After commercial products (S++ Simulation Services, Germany) for mapping current density became available, they have been used for open-cathode fuel cell performance analysis [7,8], fractal flow-field evaluation [9], starvation caused degradation [10] and comparison between gas flow configurations [11]. The current density distribution is affected by many factors, including cell design [5,12–18] and operating conditions [19–24], such as flow rate, local humidity, cell temperature, and pressure drop. For instance, the effect of cathode flow rate, humidity and cell temperature on the pattern of current density distribution was investigated by Natarajan et al. [19]. The airflow rate dominates the current density distribution, and the current density along the flow direction also increases with the airflow rate. Temperature and humidity affect the current density distribution by changing the reaction kinetics and water removal capacity. The current density increases along the flow channel under high temperatures (80 °C) and flow rates (500 sccm) because the electrolyte gradually dries out, which is verified from the measurements in a single cell with 4 cm × 12 cm active area [20]. Hartnig et al. [21] further studied the coupled electro-hydration effect via combined current density mapping and neutron radiography. They concluded that improper water management at the inlet and outlet of the anode flow field leads to uneven current density distribution during high current load.

Uneven distribution of current density and its redistribution after the operation could lead to early localised ageing of the membrane electrode assembly (MEA); the early degraded region could compromise the durability of the entire cell [12,25]. Therefore, the homogenous distribution of current density suggests that the whole activation region can be evenly utilised, thus alleviating local degradation. Firstly, chemical methods were used to achieve uniform distribution. Santis et al. [13] increased the catalyst loading along the cathode channel to compensate for the decreased oxygen concentration. A catalyst redistribution with a steeper profile suits lower cathode stoichiometries, while a smoother profile should be introduced for higher cathode stoichiometries. Secondly, the MEA structure and related flow field design have also been extensively studied to improve the non-uniform current distribution. For example, the in-plane electrical resistivity of the gas diffusion layer (GDL) has an adverse impact on current density, which is explained by the model developed by Bapat et al. [15]. Zhang et al. [18] proposed to increase GDL porosities along the cathode flow channel to maximise the availability of reactants to the catalytic site. Hsieh et al. [14] also proved that the interdigitated arrangement provides the most uniform current density distribution among all other flow field designs. [26,27].

Moreover, The relationship between temperature and current density distribution has been widely investigated; Wilkinson et al. [28] deduced the relationship between current density and temperature derivative. They developed an indirect method for measuring current density distribution using some easy-to-set-up K-type thermocouples. The local distribution of current density directly represents the local electrochemical reaction rate and thus determines the local temperature change because of one dominant electrochemical reaction, which affects the overall reaction kinetics and water management. For instance, a low current density in a local region could show cumulative deficits over time because of less heat generation.

To the best of our knowledge, the effect of the active change of local temperature on current density distribution has not been studied due to the complexity of hardware design and experimental setup. In this work, nine Peltier devices with independent temperature control have been integrated into a PEFC with 100 cm<sup>2</sup> active area, using electro-thermal mapping to investigate the relationship between active local heating and cell performance. For the first time, the nonuniform compensation of the current density distribution through real-time adjustment of operating conditions has been demonstrated. Exploring and controlling local heating helps us better understand the cell's physical mechanism and provides practical guidance for thermal management R&D. In addition,

this method can be applied to simulate local hot spots and induce degradation in a controlled manner that allows for the accurate analysis of localised faults within fuel cell stacks.

## 2. Experimental setup and procedure

### 2.1. System configuration

The experimental setup consists of three subsystems to allow for imposing local heating and measuring local current and temperature. The first implements the Peltier devices' temperature control and safety monitoring. Fig. 1(A) demonstrates the Peltier plate with its holder integrated into the fuel cell, placed directly between the flow field plate and the endplate at the anode and then measuring the electro-thermal responses on the cathode side, as the active heating and S++ plate cannot be placed on the same side, and we are more concerned with the cathode side performance. One side of the Peltier plate is an array (3 × 3) of nine independent Peltier devices with independent temperature control. The other side of the plate features a coolant flow field designed explicitly for the Peltier devices. The Peltier device in use is TE-127-1.0-0.8 from TE Technology, Inc. The length, width and height are 30 ± 0.5/−0.2 mm, 30 ± 0.5/−0.2 mm and 3.1 ± 0.05 mm, respectively. Each Peltier has independent temperature control through feedback from the thermistor and an extra thermocouple (T type) to monitor the performance and failure. A constant input voltage of 14 V is supplied to the working Peltier device, allowing the controller to determine the draw current via a PID control loop. Silicone thermal grease (RS S606C, 5 W/m·K) is applied to both sides of each Peltier device for better heat conduction and electrical insulation.

The second subsystem is the fuel cell test and data acquisition system, in which the single fuel cell studied was an in-house built system with an active area of 100 cm<sup>2</sup> and operated on a Greenlight G60 (Greenlight Innovation, USA). The hot-pressed MEA consists of commercial gas diffusion electrodes (HyPLAT) with a Pt loading of 0.4 mg cm<sup>−2</sup> and a 15 μm thick membrane (M820.15, GORE), and the electrodes employ a Freudenberg H23C9 carbon paper with MPL (Freudenberg, Germany) and a hydrophobic treatment [29]. The flow field configuration was a 7-channel serpentine with a land width and channel depth and width of 1 mm. The plate on the anode side is 2 mm aluminium that is gold-coated to maintain an active temperature gradient after transfer to the MEA position, and 6 mm graphite is used on the cathode side. The mapping instrument, consisting of 7 × 7 temperature and 14 × 14 current density measurements integrated into a PCB plate (S++ Simulation Services), was placed between the current collector and the flow field plate at the cathode. The temperature mapping measures the active local temperature control and spatially correlates to the local current density distribution for performance changes. The cell assembly was sealed with a torque of 3 Nm applied to the 12 bolts, and the pressure distribution mapping in the active area region can be found in Fig. S1. More details about the cell assembly and components can be found in previous work by Rasha et al. [11]. The third subsystem is the customised coolant control system, which controls the temperature and flow rate of the circulating coolant.

### 2.2. Experimental conditions

Due to the non-uniform distribution of reactant concentration and local relative humidity (RH) from the inlet to the outlet along the flow field, local heating was carried out at the cathode inlet (device 1), middle (device 5) and outlet (device 9) of the single cell separately. The configuration of the flow field arrangement and the heating area is shown in Fig. 1(B). The temperature of the hot side of the Peltier device is set at 60 °C, and the temperature offset is generated when a current is applied across two materials, called the Peltier effect. Moreover, the temperature of the coolant is kept at 40 °C. The sampling interval for all equipment is the same (0.2 s) for data consistency.

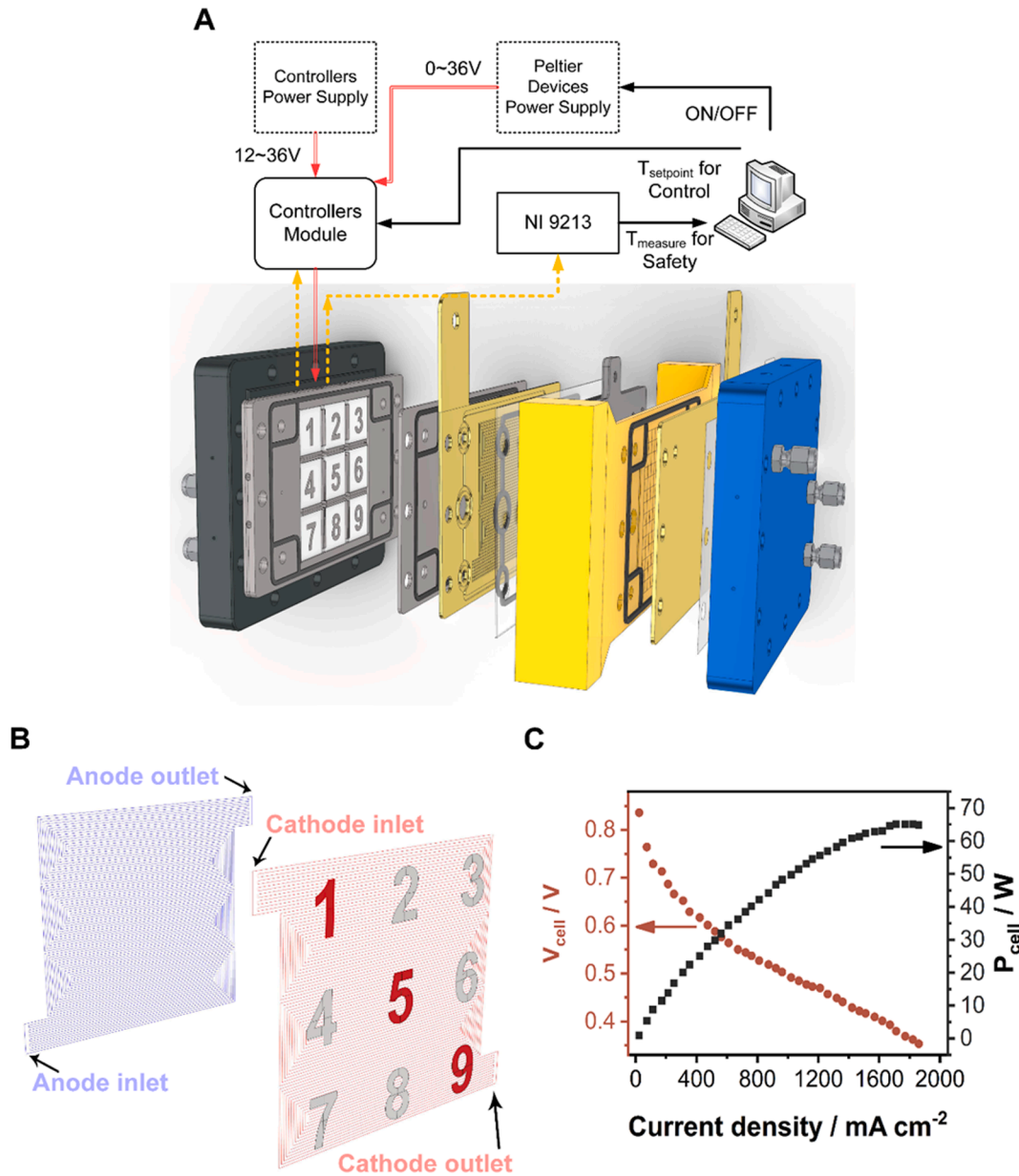


**Fig. 1.** (A) The single-cell system configuration to realise local heating. (B) Local heating location and flow configuration. (C) Cell performance without local heating (70% RH); coolant temperature is set to 40 °C.

The operating conditions are listed in Table 1, and the inlet RH is calculated according to the cell operating temperature of 40 °C and the temperature of the fed gases. As the overall cell output is shown in Fig. 1 (C), analysis of the current density distribution and temperature distribution under mass transport controlled ( $j = 1300 \text{ mA cm}^{-2}$ ), Ohmic ( $j = 750 \text{ mA cm}^{-2}$ ) and activation ( $j = 200 \text{ mA cm}^{-2}$ ) ‘global’ current densities were undertaken to assess the effect of local heating on current distribution and, therefore, fuel cell performance.

**Table 1**

The operating conditions of the single cell.

Operation parameter	Nominal value
RH (Cathode/Anode)	0%, 70% and 100%
Pressure (Cathode/Anode)	0 kPa
Stoichiometry (Anode)	1.5
Stoichiometry (Cathode)	3
Coolant inlet temperature	40 °C

### 3. Results and discussion

#### 3.1. Activation region

To verify the causal relationship between local heating and current density change, it is necessary to calculate the correlation coefficient between them. Eq. (1) is used to calculate the 2-D correlation coefficient [30] between two matrixes.

$$r = \frac{\sum_{i=1}^m \sum_{j=1}^n (p_{ij} - \bar{p})(q_{ij} - \bar{q})}{\sqrt{[\sum_{i=1}^m \sum_{j=1}^n (p_{ij} - \bar{p})^2][\sum_{i=1}^m \sum_{j=1}^n (q_{ij} - \bar{q})^2]}} \quad (1)$$

In which The  $p_{ij}$  and  $q_{ij}$  are the pixel value at  $i^{\text{th}}$  row and  $j^{\text{th}}$  column respectively,  $\bar{p}$  and  $\bar{q}$  are average pixel value, and the size of each matrix is  $m \times n$ . Considering that the  $7 \times 7$  temperature distribution measurement and  $14 \times 14$  current distribution measurement are over the same area, upsampling should be performed to the temperature distribution by the method called Nearest Neighbor, shown in Fig. 2(A), which

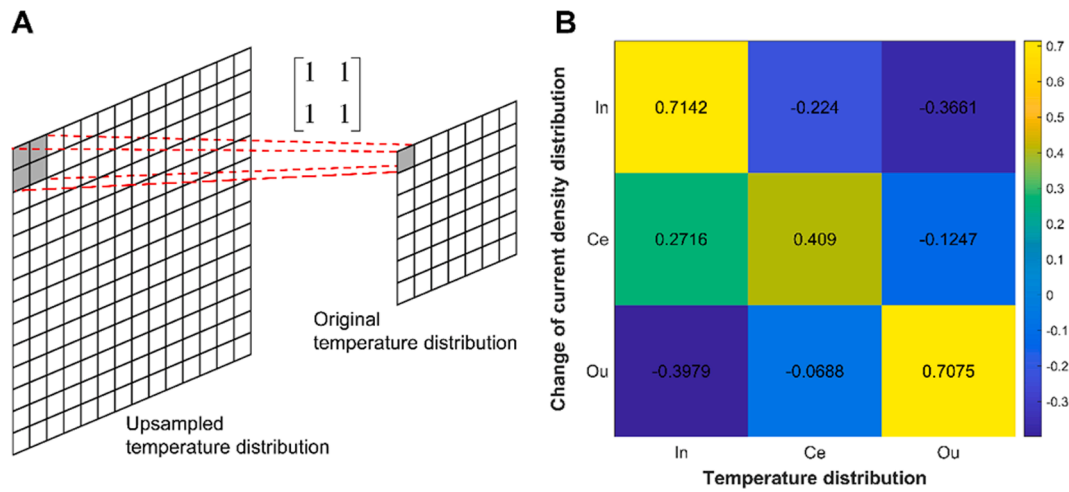


**Fig. 2.** (A) Schematic representation of the temperature distribution upsampling process. (B) The correlation coefficient matrix between current density distribution change and temperature distribution for the activation region ( $j = 200 \text{ mA cm}^{-2}$ , 70% RH). In, Ce and Ou represent inlet, central and outlet area heating, respectively.

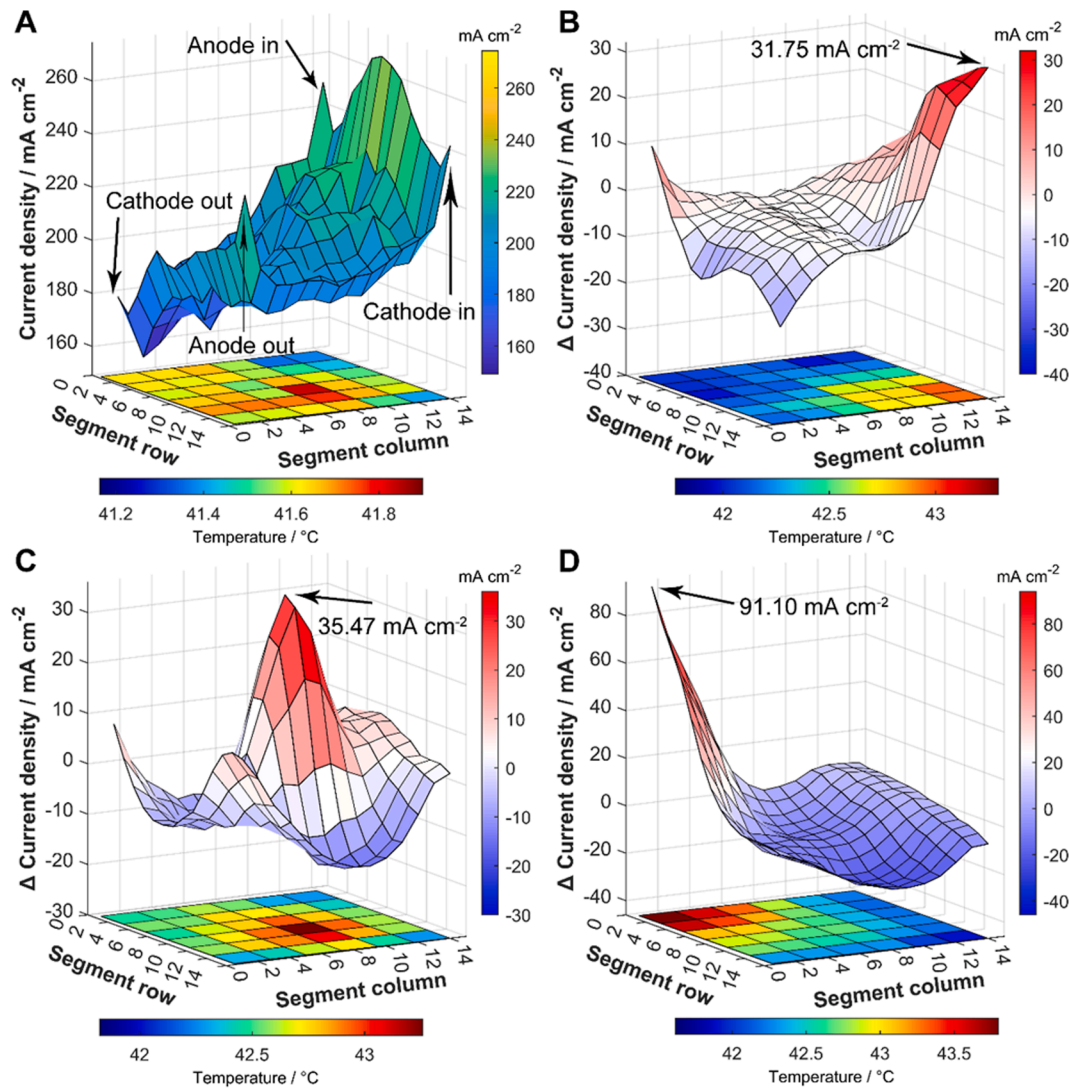


**Fig. 3.** The corresponding current density distribution (vertical axis, blue-red colour gradient) and temperature distribution (base plane, rainbow colour gradient) for (A) the activation region ( $j = 200 \text{ mA cm}^{-2}$ ) without local heating (70% RH). (B–D) The change of current density distribution (compared to no heating) and temperature distribution corresponds to the activation region during inlet (B), central (C) and outlet (D) heating, respectively (70% RH).



copies a pixel value of the input map to all pixels in the corresponding sub-region of output. Then, the correlation coefficients ( $r$ ) can be calculated. The value of  $r$  is between  $-1$  and  $1$ .

The 2-D correlation coefficient matrix depicted in Fig. 2(B) reveals that the highest correlation coefficient can be obtained when the region of the current density change corresponds to the region of local heating. For example, the current density distribution change for the inlet area heating has the highest correlation coefficient with the temperature distribution caused by inlet heating, which is  $0.7142$ . In general, the area of local heating (inlet, outlet, central) correlates most strongly with the current density distribution in the area matching that heating, proving that the increase in local current density is due to the local heating itself.

Fig. 3(A) presents the current density and temperature distribution for a coolant-controlled temperature of  $40^\circ\text{C}$  in the activation region ( $j = 200\text{ mA cm}^{-2}$ ), where none of the Peltier devices is active. In all these figures, the cathode inlet is situated at  $(14,14)$  in the base panel coordinates, and the cathode outlet at  $(0,0)$ ; the anode inlet and outlet are situated at  $(0,14)$  and  $(14,0)$ , respectively (labelled on Fig. 3(A)). Overall, the current density distribution at the cathode inlet is higher than at the outlet, and the same trend is evident for hydrogen flow. Fig. 3 (B)-(D) show the temperature distribution and current density changes (minus the 'baseline' current density distribution of Fig. 3(A)) during

local heating in three different areas. In the activation region, the cell generates less heat due to the higher efficiency of the fuel cell at low currents. The cooling water temperature at the outlet and inlet is nearly the same (Fig. S7(A)). The corresponding local current density increases when the local temperature increases due to local heating provided by the Peltier array. When the temperature at the inlet area increases, the current density increases by  $31.75\text{ mA cm}^{-2}$  at most. When the local heating occurs in the central area, the current density increases by  $35.47\text{ mA cm}^{-2}$ . The largest current density increase for the outlet area temperature increase is  $91.10\text{ mA cm}^{-2}$ , corresponding to a  $1.28\%$  output voltage improvement. This means that areas with higher current density are alleviated, and the overall reaction occurs more evenly.

The frequency analysis of current density distribution corresponding to the activation region ( $j = 200\text{ mA cm}^{-2}$ ) without or with local heating is shown in Fig. S2, where the x-axis represents current density and the y-axis represents the counts of current density pixels in a particular range. Ideally, the current density is evenly distributed, and all pixels should fall at the  $200\text{ mA cm}^{-2}$  point (the 'global' current density defined by the load). Compared with other heating operations, the distribution (more concentrated) is closer to the ideal one under the condition of outlet heating, so cell performance improves accordingly.

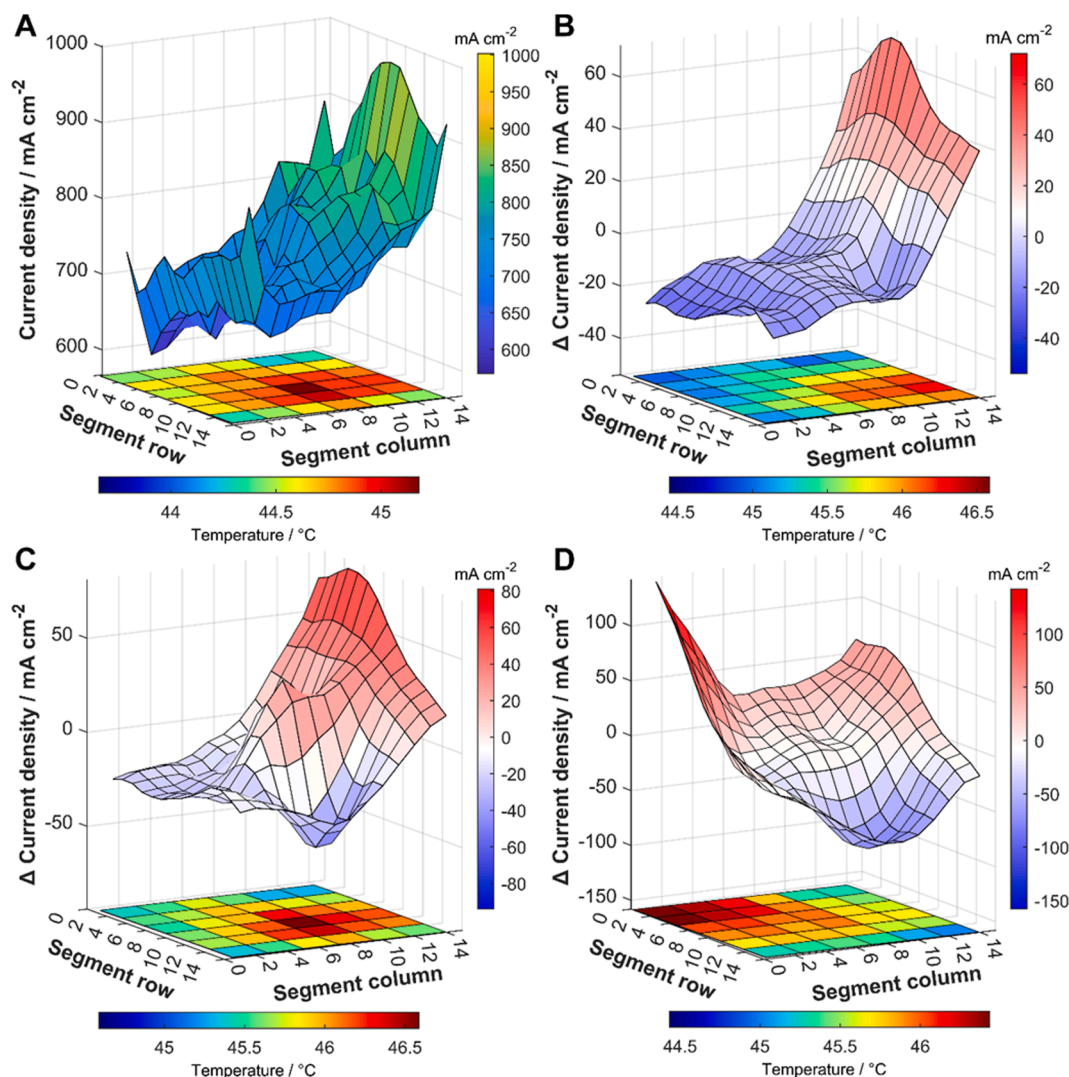


**Fig. 4.** (A) The corresponding current density and temperature distribution in the Ohmic region ( $j = 750\text{ mA cm}^{-2}$ ) without local heating (70% RH). (B-D) The change of current density distribution (compared to no heating) and temperature distribution corresponds to the Ohmic region during inlet (B), central (C) and outlet (D) heating, respectively (70% RH).

### 3.2. Ohmic region

In the Ohmic region ( $j = 750 \text{ mA cm}^{-2}$ ), the increased flow of ions and electrons leads to a more significant voltage loss than in the activation region, with a large amount of heat generated. In Fig. 4(A), the maximum temperature increased to  $45.2^\circ\text{C}$  compared to  $41.9^\circ\text{C}$  in the activation region under no local heating. Furthermore, the coolant outlet temperature also slightly increased to  $40.4^\circ\text{C}$  (Fig. S7(B)), which means the coolant is working to remove the heat, so the effect of local heating on cell performance changes accordingly. For both inlet and central heating, the area of larger current density when no local heating is applied continues to increase (Fig. 4(B) and (C)), even when accounting for normalisation to the baseline case without heating. In the case of central local heating, an additional, more minor, increase in current density is detected in the centre of the cell. Besides, the maximum current density (as shown in Fig. S3(B) and S3C) and the standard deviation continued to increase, so it can be concluded that improper local heating will worsen the uneven current density distribution. It can also be found from Fig. S5 that the region where the current density changes and the local heating region no longer always match. The effect of outlet heating on current density is pronounced, with the current density in the heating area increasing by  $143 \text{ mA cm}^{-2}$ .

The large relative increase in the outlet region serves to produce the most even distribution of current density for this case, compensating for the uneven current density that arises without local heating. The shift of current density to a lower range can be found in Fig. S3(D), corresponding to a 2.17% output voltage improvement. In this way, providing local heating to the outlet region of the fuel cell balances the current density distribution across the MEA for the medium current operation ( $750 \text{ mA cm}^{-2}$  global current density).

### 3.3. Mass transport controlled region

For the mass transport controlled region ( $j = 1300 \text{ mA cm}^{-2}$ ) and no local heating case, the maximum temperature in the active area reached  $49.8^\circ\text{C}$  (Fig. 5(A)), corresponding to a high current density which is around  $1415 \text{ mA cm}^{-2}$  (excluding the edges). In contrast to the lower current density cases (activation and Ohmic regions of the polarisation curve), at high current density, the heat generated by the fuel cell reaction itself tends to dominate the area of local heating (located around the centre and inlet), such that in the cases where additional local heating is supplied it either enhances the existing hotspot or adds a different hotspot in an adjacent area, as shown in Fig. 5(B)–(D). Under all the local heating cases, a hotspot appears in the central region. For

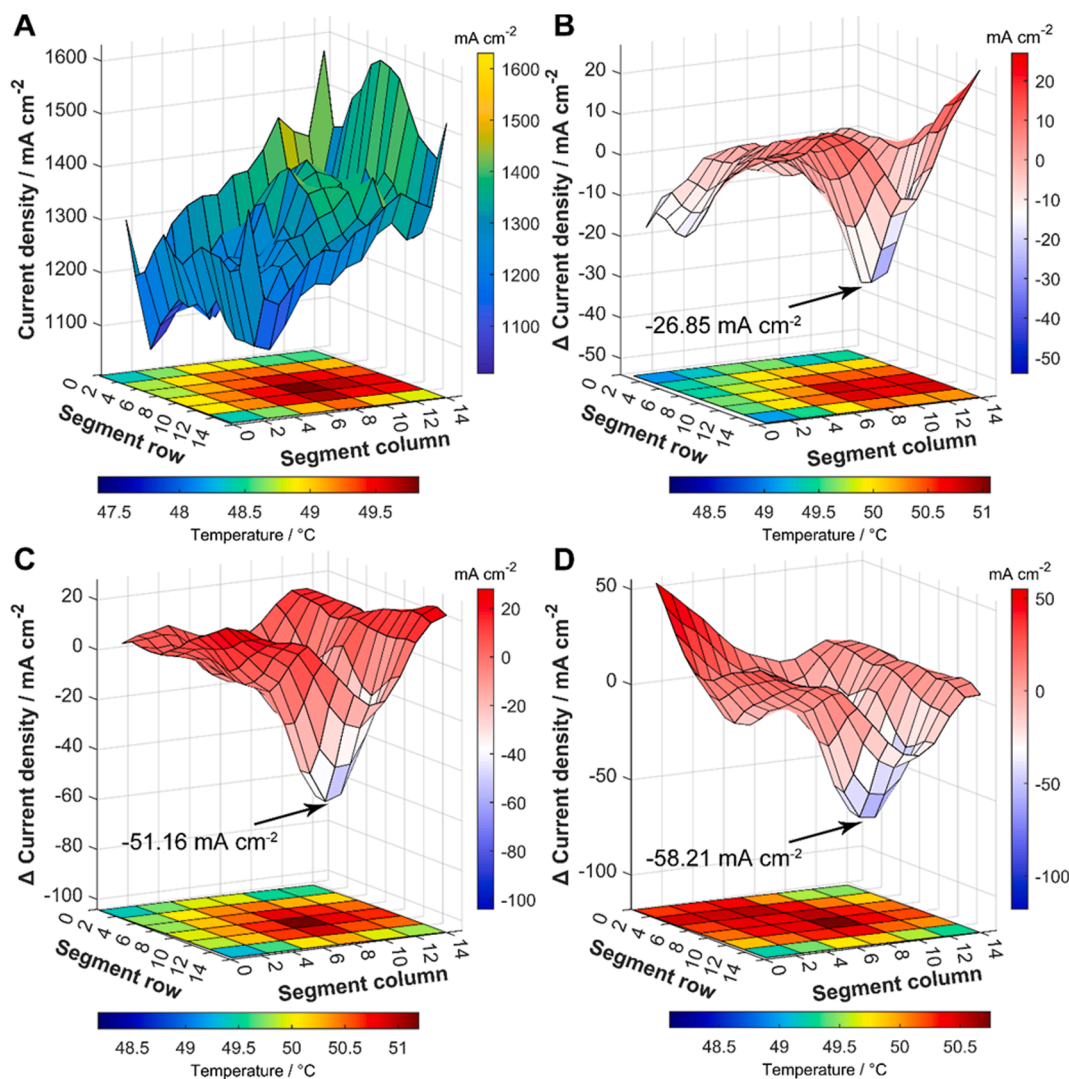


**Fig. 5.** (A) The corresponding current density and temperature distribution in the mass transport controlled region ( $j = 1300 \text{ mA cm}^{-2}$ ) without local heating (70% RH). (B–D) The change of current density distribution (compare to no heating) and temperature distribution corresponds to mass transport controlled region during inlet (B), central (C) and outlet (D) heating (70% RH).

example, the maximum temperature in the active area reached up to 51.2 °C in the central heating case. This results in a drop in current density in the central active area, and excessive temperatures may adversely affect local water management.

Although water uptake is enhanced with increasing temperature, there exists a trade-off between water uptake and membrane dehydration. Therefore, the water content in the membrane will decrease with the elevated operating temperature [31] once the balance is broken. Uneven current density can arise across the area of the MEA for many reasons [32], leading to uneven heating. By implementing local heating in various positions in the cell, we aim to counter the variation across the cells and produce a more even distribution of current, which could lead to lower degradation and maximised utilisation of the MEA. In the mass transport controlled region, as with the activation and Ohmic region,

local heating at the outlet acts to more evenly distribute the current density than in the case with no local heating; however, due to the increased contribution from the electrochemical reaction to the overall heating of the fuel cell, in which the coolant outlet temperature is around 41.2 °C (Fig. S7(C)), local heating at this current density has a less effective result in balancing the current density, with local cooling likely to provide a more even current distribution across the MEA.

As shown in Fig. 6(D)–(F), the minimum and maximum temperatures increase for all local heating configurations compared to no local heating, which indicates that the local heat passes through the covering plate and the flow field plate and simultaneously transmits across the plane, thus increasing the overall temperature of the cell. For all heating cases, the temperature differences are around 1–3 °C. It is also worth mentioning that the temperature differences at the MEA should be

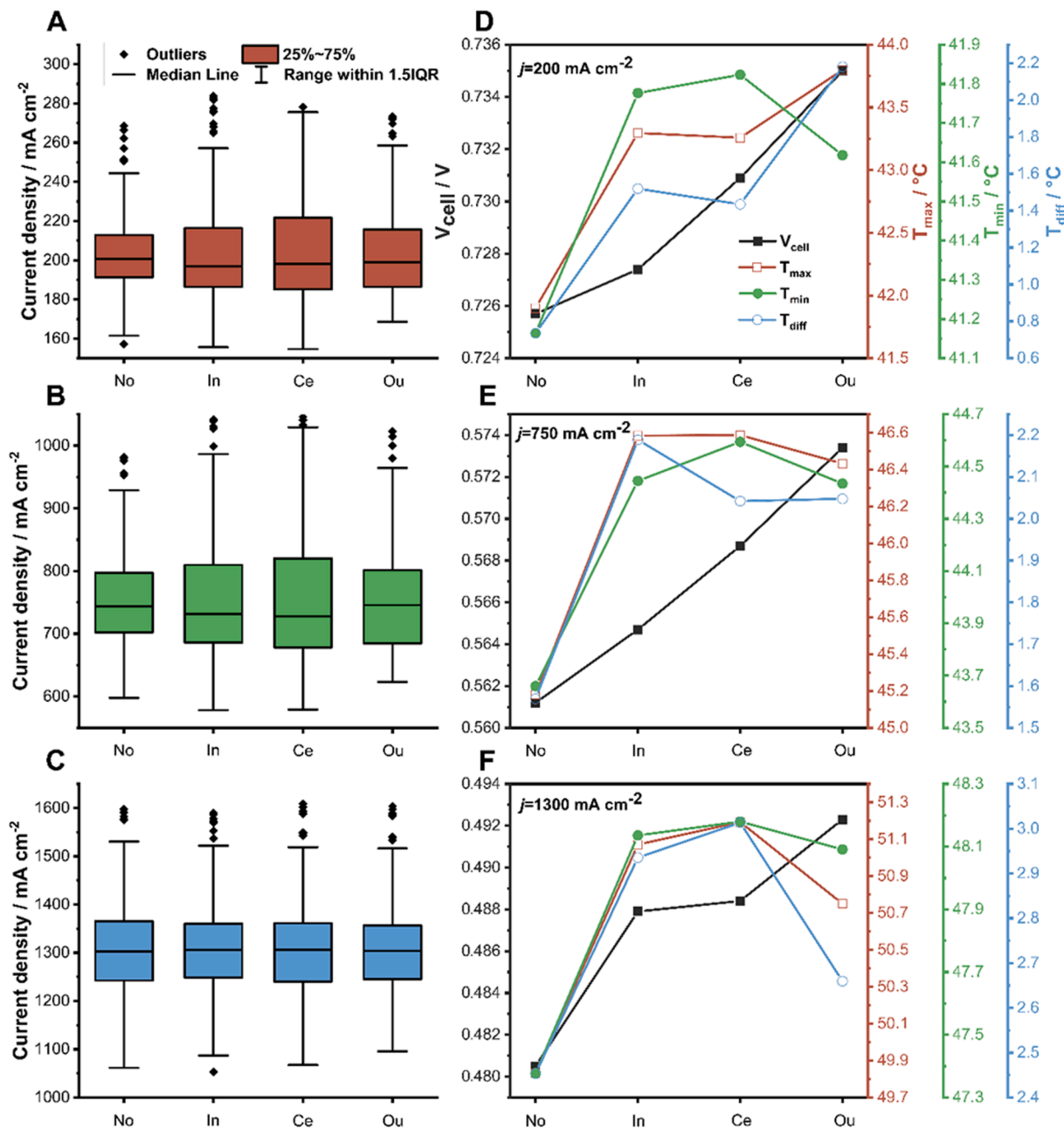


**Fig. 6.** (A–C) Maximum ( $T_{\text{max}}$ ), minimum ( $T_{\text{min}}$ ) temperature and temperature difference ( $T_{\text{diff}}$ ) for activation region ( $j = 200 \text{ mA cm}^{-2}$ , A), Ohmic region ( $j = 750 \text{ mA cm}^{-2}$ , B) and mass transport controlled region ( $j = 1300 \text{ mA cm}^{-2}$ , C). (D–F) Cell voltage (V) at 70% RH, current density standard deviation ( $\text{CD}_{\text{std}}$ ), minimum ( $\text{CD}_{\text{min}}$ ) and maximum ( $\text{CD}_{\text{max}}$ ) current density distribution for activation region (D), Ohmic region (E) and mass transport controlled region (F) at 70% RH. No represents no local heating, In, Ce, and Ou represent inlet, central and outlet area heating, respectively.

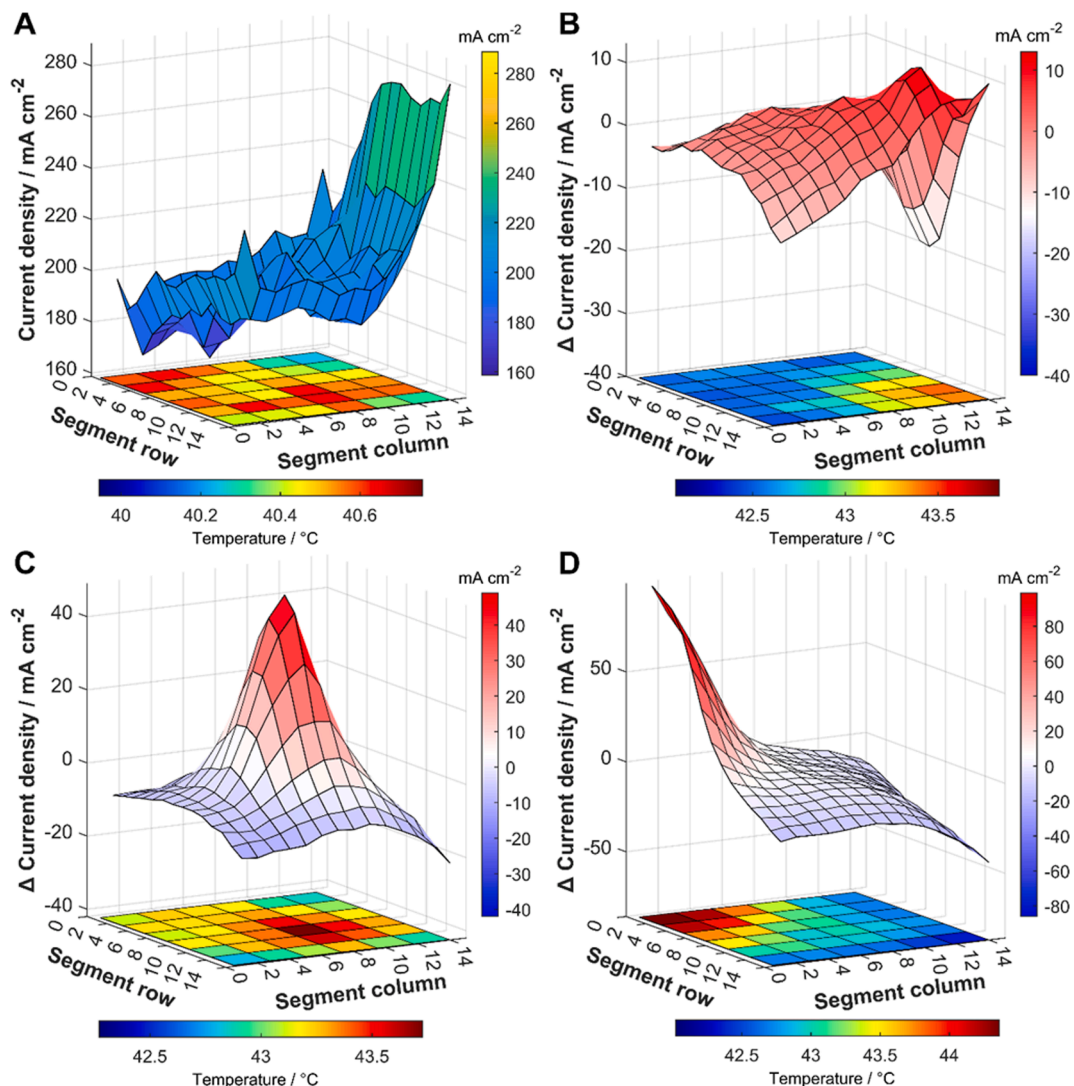


**Fig. 7.** (A) The corresponding current density and temperature distribution in the activation region without local heating (100% RH). (B–D) The change of current density distribution (compared to no heating) and temperature distribution correspond to the activation region during inlet (B), central (C) and outlet (D) heating (100% RH).

higher as the active thermal gradient is transferred first to the MEA and then to the S++ current collection plate. The locations of the observed hot spots (Fig. 3(B)–(D)) also indicate the effectiveness of local heating. In all heating cases, the performance improvement is attributed to the influence of current density distribution; the combination of the decrease in maximum current density, the increase of minimum current density, and the reduction of current density standard deviation (Fig. 6 (A)–(C)) will result in a more uniform reaction and higher output voltage. In the mass transport controlled region, it is clear that the current density distribution for heating cases is similar to no heating; achieving local cooling should be considered as the cell generates lots of heat.

As the average temperature of the cell increases, performance increases for all cases at each current density (70% RH). The local heating carried out in inlet, middle and outlet locations affects fuel cell performance differently. Generally, the cell performs best when heated locally at the outlet position (here, we are only comparing different heating positions), whether in the activation, Ohmic, or mass transport controlled regions of the polarisation curve. Mass transfer resistance can be reduced for higher temperatures by improving condensation problems, reducing the amount of liquid water and enhancing the catalytic activity [31]. In addition, the membrane's water adsorption capacity

and ionic conductivity are enhanced [33] as long as the humidification is sufficient and the membrane remains hydrated everywhere.

### 3.4. Effect of Relative Humidity

Local heating affects the reaction kinetics and may change local water management. The external characteristics of the cell are shown in Table 2. By comparing the voltage of outlet area heating with that of no local heating, the cell voltage increases from 0.7257 V to 0.7350 V (1.38%) at 70% relative humidity (RH). The voltage rises from 0.6845 V to 0.7156 V (4.54%) at 100% RH without and with local heating. In the case of no humidification (RH = 0%), the voltage jumped from 0.6832 V to 0.7303 V (6.9%). It seems that local heating has the most acute effect on the local voltage under no humidification, indicating that improved water management is not the main reason for local heating improving the performance of the fuel cell.

At 100% RH, as shown in Fig. 7(A), the current density distribution reaches its highest point near the reaction gas inlet, which results from the least amount of liquid water accumulated at the inlet area. After changing the local temperature, the current density distribution did not change dramatically (Fig. 7(B)–(D)) compared to the 70% RH cases discussed in Fig. 3. It suggests that local heating does not improve



**Table 2**

Cell voltage (V) in activation region for different RH, none represents no local heating.

	70% RH	100% RH	0% RH
None	0.7257	0.6845	0.6832
Inlet	0.7274	0.7071	0.7143
Central	0.7309	0.7127	0.7253
Outlet	0.7350	0.7156	0.7303

performance primarily through improved water management but through changing reaction kinetics. The results obtained without humidification also validate this conclusion (Fig. 8) since the shapes and distribution trends of the current density and temperature distribution plots corresponding to the activation region at the cathode inlet, central and outlet are similar when we compare the Fig. 7(B)–(D) (RH = 100%) to Fig. 8(B)–(D) (RH = 0%). The local heating can still change the current density distribution, even if the reactants are dried out, and the cell does not generate much water in the activation region.

#### 4. Conclusions

This work integrated a Peltier array with independent temperature

control into a commercial-sized PEFC with a 100 cm<sup>2</sup> active area. The electro-thermal mapping was used to investigate the effect of active local heating on cell performance. Local heating was used to compensate for non-uniform current density distributions across the MEAs of PEFCs. Generally, the fuel cell does not produce sufficient heat in the activation region. In the local area, the heating increases current density at the associated location of the cathode (inlet, central and outlet). In particular, it is expected to obtain the highest output voltage among all heating locations when heating is applied to the outlet due to the homogeneous current density distribution via local current compensation. Specifically, the largest current density was increased by 91.10 mA cm<sup>-2</sup> at the outlet area, the highest among all locations. The Ohmic region has a similar trend to the previous region. When it comes to the mass transport region, it is found that the local heating has limited influence on the outlet area, as the heat production of the cell itself mainly dominates the temperature distribution in the active area. This is because the higher local temperature might dry up the membrane (for inlet, central heating and outlet heating, the largest decrease of current densities was 26.9, 51.1 and 58.2 mA cm<sup>-2</sup> according to local hot spots).

The results suggest introducing coolant to lower current density areas to provide local heating if coolant temperature exceeds the cell, and to high current density areas for extra cooling. Continuous

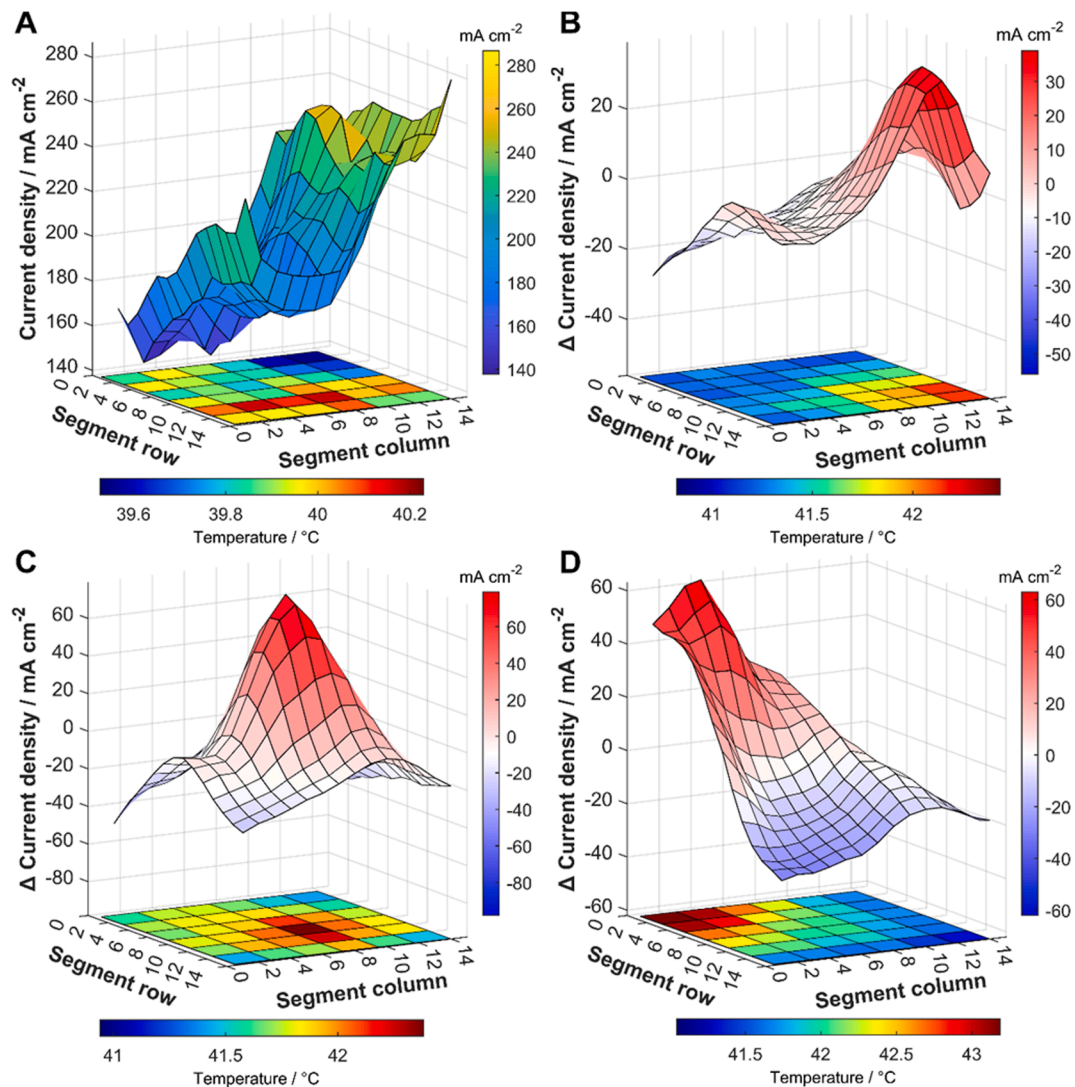


**Fig. 8.** (A) The corresponding current density and temperature distribution in the activation region without local heating (0%RH). (B–D) The change of current density distribution (compared to no heating) and temperature distribution correspond to the activation region during inlet (B), central (C) and outlet (D) heating (0%RH).

monitoring and adjustment of coolant flow based on temperature and current density distribution is crucial. Flexible fuel cell designs accommodating these changes could enhance PEFC efficiency and mitigate local degradation. Our research provides a feasible route to modify the dynamic design of thermal management systems and thus improve the understanding of cell behaviours.

### CRedit authorship contribution statement

**Shangwei Zhou:** Conceptualization, Methodology, Formal analysis, Investigation, Data curation, Writing – original draft, Writing – review & editing, Visualization. **Lara Rasha:** Investigation, Visualization, Writing – original draft, Writing – review & editing. **Linlin Xu:** Data curation, Visualization, Writing – review & editing. **Wenjia Du:** Writing – original draft, Writing – review & editing. **Paul R. Shearing:** Resources, Writing – review & editing, Funding acquisition. **Marc-Olivier Coppens:** Resources, Writing – review & editing, Supervision, Funding acquisition. **Dan J.L. Brett:** Resources, Writing – review & editing, Supervision, Funding acquisition. **Rhodri Jervis:** Conceptualization, Resources, Writing – original draft, Writing – review & editing, Supervision, Project administration, Funding acquisition.

### Declaration of Competing Interest

The authors declare that they have no known competing financial interests or personal relationships that could have appeared to influence the work reported in this paper.

### Data availability

Data will be made available on request.

### Acknowledgements

SZ acknowledges the Chinese Scholarship Council [grant number: 202108060113] and BRAMBLE ENERGY LIMITED for funding support of his PhD. LX acknowledges the Engineering and Physical Sciences Research Council [grant number EP/N509577/1, EP/T517793/1] for funding support of her PhD. LR acknowledges the financial support by the Faraday Institution [EP/S003053/1, grant number: FIRG015]. DB/PRS acknowledge the EPSRC for funding fuel cell research in the EIL (EP/L015277/1, EP/P009050/1, EP/M014371/1, EP/M009394/1, EP/M023508/1, EP/L015749/1, EP/N022971/1) and the Royal Academy of Engineering for supporting the Research Chairs of DB (RCSRF2021/13/53) and PRS (CiET1718/59). MOC is grateful to the EPSRC for funding via a “Frontier Engineering: Progression” grant (EP/S03305X/1). This project was supported by the Royal Academy of Engineering under the Research Chairs and Senior Research Fellowships scheme.

### Appendix A. Supplementary data

Supplementary data to this article can be found online at <https://doi.org/10.1016/j.enconman.2023.117717>.

### References

- [1] Zhou S, Shearing PR, Brett DJ, Jervis R. Machine learning as an online diagnostic tool for proton exchange membrane fuel cells. *Curr Opin Electrochem* 2022;31: 100867.
- [2] Islam MR, Shabani B, Rosengarten G. Nanofluids to improve the performance of PEM fuel cell cooling systems: A theoretical approach. *Appl Energy* 2016;178: 660–71.
- [3] Suter TA, Smith K, Hack J, Rasha L, Rana Z, Angel GMA, et al. Engineering catalyst layers for next-generation polymer electrolyte Fuel cells: a review of design, materials, and methods. *Adv Energy Mater* 2021;11:2101025.
- [4] Jiang Y, Huang L, Zhang X, Rasha L, Brett DJ. Proton exchange membrane fuel cell performance investigation considering internal heterogeneity of current density—a novel method study. *Int J Hydrogen Energy* 2022;47:20205–17.
- [5] Hwnag J, Chang W, Peng R, Chen P, Su A. Experimental and numerical studies of local current mapping on a PEM fuel cell. *Int J Hydrogen Energy* 2008;33:5718–27.
- [6] Yu Y, Yuan X-Z, Li H, Gu E, Wang H, Wang G, et al. Current mapping of a proton exchange membrane fuel cell with a segmented current collector during the gas starvation and shutdown processes. *Int J Hydrogen Energy* 2012;37:15288–300.
- [7] Meyer Q, Ashton S, Jervis R, Finegan DP, Boillat P, Cochet M, et al. The hydro-electro-thermal performance of air-cooled, open-cathode polymer electrolyte fuel cells: combined localised current density, temperature and water mapping. *Electrochim Acta* 2015;180:307–15.
- [8] Meyer Q, Ronaszegi K, Robinson J, Noorkami M, Curnick O, Ashton S, et al. Combined current and temperature mapping in an air-cooled, open-cathode polymer electrolyte fuel cell under steady-state and dynamic conditions. *J Power Sources* 2015;297:315–22.
- [9] Bethapudi V, Hack J, Hinds G, Shearing P, Brett D, Coppens M-O. Electro-thermal mapping of polymer electrolyte membrane fuel cells with a fractal flow-field. *Energy Convers Manage* 2021;250:114924.
- [10] Yezerska K, Dushina A, Liu F, Rastedt M, Wagner P, Dyck A, et al. Characterisation methodology for anode starvation in HT-PEM fuel cells. *Int J Hydrogen Energy* 2019;44:18330–9.
- [11] Rasha L, Cho J, Millichamp J, Neville T, Shearing P, Brett D. Effect of reactant gas flow orientation on the current and temperature distribution in self-heating polymer electrolyte fuel cells. *Int J Hydrogen Energy* 2021;46:7502–14.
- [12] Miao T, Tongsh C, Wang J, Cheng P, Liang J, Wang Z, et al. Current density and temperature distribution measurement and homogeneity analysis for a large-area proton exchange membrane fuel cell. *Energy* 2022;239:121922.
- [13] Santis M, Freunberger SA, Reiner A, Büchi F. Homogenization of the current density in polymer electrolyte fuel cells by in-plane cathode catalyst gradients. *Electrochim Acta* 2006;51:5383–93.
- [14] Hsieh S-S, Huang Y-J. Measurements of current and water distribution for a micro-PEM fuel cell with different flow fields. *J Power Sources* 2008;183:193–204.
- [15] Bapat CJ, Thynell ST. Effect of anisotropic electrical resistivity of gas diffusion layers (GDLs) on current density and temperature distribution in a Polymer Electrolyte Membrane (PEM) fuel cell. *J Power Sources* 2008;185:428–32.
- [16] Lobato J, Canizares P, Rodrigo MA, Pinar FJ, Úbeda D. Study of flow channel geometry using current distribution measurement in a high temperature polymer electrolyte membrane fuel cell. *J Power Sources* 2011;196:4209–17.
- [17] Zhang Y, Smirnova A, Verma A, Pitchumani R. Design of a proton exchange membrane (PEM) fuel cell with variable catalyst loading. *J Power Sources* 2015; 291:46–57.
- [18] Zhang Y, Verma A, Pitchumani R. Optimum design of polymer electrolyte membrane fuel cell with graded porosity gas diffusion layer. *Int J Hydrogen Energy* 2016;41:8412–26.
- [19] Natarajan D, Van Nguyen T. Current distribution in PEM fuel cells. Part 2: Air operation and temperature effect. *AIChE J* 2005;51:2599–608.
- [20] Brett D, Atkins S, Brandon N, Vasileiadis N, Vesovic V, Kucernak A. Membrane resistance and current distribution measurements under various operating conditions in a polymer electrolyte fuel cell. *J Power Sources* 2007;172:2–13.
- [21] Hartnig C, Manke I, Kardjilov N, Hilger A, Grünerbel M, Kaczerowski J, et al. Combined neutron radiography and locally resolved current density measurements of operating PEM fuel cells. *J Power Sources* 2008;176:452–9.
- [22] Jeon DH, Kim KN, Baek SM, Nam JH. The effect of relative humidity of the cathode on the performance and the uniformity of PEM fuel cells. *Int J Hydrogen Energy* 2011;36:12499–511.
- [23] Zhang G, Shen S, Guo L, Liu H. Dynamic characteristics of local current densities and temperatures in proton exchange membrane fuel cells during reactant starvations. *Int J Hydrogen Energy* 2012;37:1884–92.
- [24] Zhang G, Wu J, Wang Y, Yin Y, Jiao K. Investigation of current density spatial distribution in PEM fuel cells using a comprehensively validated multi-phase non-isothermal model. *Int J Heat Mass Transf* 2020;150:119294.
- [25] Peng L, Shao H, Qiu D, Yi P, Lai X. Investigation of the non-uniform distribution of current density in commercial-size proton exchange membrane fuel cells. *J Power Sources* 2020;453:227836.
- [26] Xing L, Wang Y, Das PK, Scott K, Shi W. Homogenization of current density of PEM fuel cells by in-plane graded distributions of platinum loading and GDL porosity. *Chem Eng Sci* 2018;192:699–713.
- [27] Wang Y, Xu H, Wang X, Gao Y, Su X, Qin Y, et al. Multi-sub-inlets at cathode flow-field plate for current density homogenisation and enhancement of PEM fuel cells in low relative humidity. *Energy Convers Manage* 2022;252:115069.
- [28] Wilkinson M, Blanco M, Gu E, Martin J, Wilkinson D, Zhang J, et al. In situ experimental technique for measurement of temperature and current distribution in proton exchange membrane fuel cells. *Electrochim Solid St* 2006;9:A507.
- [29] Zhou S, Xu L, Trogadas P, Rasha L, Du W, Shearing PR, et al. Effects of an easy-to-implement water management strategy on performance and degradation of polymer electrolyte fuel cells. *J Power Sources* 2023;575:233184.
- [30] Pradhan A, Sahu AK, Swain G, Sekhar KR. Performance evaluation parameters of image steganography techniques. In: 2016 International Conference on Research Advances in Integrated Navigation Systems. (RAINS): IEEE; 2016. p. 1–8.
- [31] Ozen DN, Timurkutluk B, Altinisik K. Effects of operation temperature and reactant gas humidity levels on performance of PEM fuel cells. *Renew Sustain Energy Rev* 2016;59:1298–306.
- [32] Tang W, Lin R, Weng Y, Zhang J, Ma J. The effects of operating temperature on current density distribution and impedance spectroscopy by segmented fuel cell. *Int J Hydrogen Energy* 2013;38:10985–91.
- [33] Coppo M, Siegel N, Von Spakovsky M. On the influence of temperature on PEM fuel cell operation. *J Power Sources* 2006;159:560–9.